Genetics inMedicine | ARTICLE

Role of *MDH2* pathogenic variant in pheochromocytoma and paraganglioma patients

Bruna Calsina, MSc, Mercedes Robledo, PhD et al.[#]

Purpose: *MDH2* (malate dehydrogenase 2) has recently been proposed as a novel potential pheochromocytoma/paraganglioma (PPGL) susceptibility gene, but its role in the disease has not been addressed. This study aimed to determine the prevalence of *MDH2* pathogenic variants among PPGL patients and determine the associated phenotype.

Methods: Eight hundred thirty patients with PPGLs, negative for the main PPGL driver genes, were included in the study. Interpretation of variants of unknown significance (VUS) was performed using an algorithm based on 20 computational predictions, by implementing cell-based enzymatic and immunofluorescence assays, and/or by using a molecular dynamics simulation approach.

Results: Five variants with potential involvement in pathogenicity were identified: three missense (p.Arg104Gly, p.Val160Met and p.Ala256Thr), one in-frame deletion (p.Lys314del), and a splice-site variant (c.429+1G>T). All were germline and those with available biochemical data, corresponded to noradrenergic PPGL.

Conclusion: This study suggests that *MDH2* pathogenic variants may play a role in PPGL susceptibility and that they might be responsible for less than 1% of PPGLs in patients without pathogenic variants in other major PPGL driver genes, a prevalence similar to the one recently described for other PPGL genes. However, more epidemiological data are needed to recommend *MDH2* testing in patients negative for other major PPGL genes.

Genetics in Medicine (2018) 20:1652–1662; https://doi.org/10.1038/s41436-018-0068-7

Keywords: *MDH2*; pheochromocytoma and paraganglioma; Variants of unknown significance; Dominant-negative effect; Molecular dynamics

INTRODUCTION

Pheochromocytoma (PCCs) and paragangliomas (PGLs), abbreviated as PPGLs, are very rare neuroendocrine tumors characterized by a high degree of genetic and clinical heterogeneity.[1,2]

Since the description of *NF1* in 1990 as the first driver gene related to PPGL development, 35 additional genes have been identified to be involved in the disease, establishing PPGLs as the human neoplasia with the highest degree of heritability. Among PPGL-associated genes, seven have been found almost exclusively mutated in the germline (*SDHA*, *SDHB*, *SDHC*, *SDHD*, *SDHAF2*, *FH*, and *TMEM127*), four either in the germline or somatically (*RET*, *VHL*, *NF1*, and *MAX*), one postzygotically or somatically (*EPAS1*), and the last one only somatically (*HRAS*).[1,3] Furthermore, there are 22 more susceptibility genes for which the contribution to the disease remains unclear: *IDH1, KIF1B, MEN1, BAP1, EGLN1/PHD2, EGLN2/PHD1, ATRX, KMT2D/MLL2, MET, TP53, BRAF, JMJD1C, KDM2B, MERTK, H3F3A, SETD2, EZH2, FGFR1, MITF*, *CSDE1*, *GOT2*, and *IDH3B*.[1,4–12] In addition, other mechanisms such as point variants in the promoter region of *TERT*,[13,14] *SDHC* promoter epimutations,[15] or rearrangements involving *MAML3, BRAF, NGFR*, and *NF1* have been also described.[11]

Recently, our group added malate dehydrogenase 2 (*MDH2*) to the list of potential PPGL susceptibility genes. *MDH2* encodes the mitochondrial malate dehydrogenase (MDH), essential for the conversion of malate to oxaloacetate as part of the proper functioning of the Krebs cycle. A single *MDH2* PV affecting a donor splice-site (c.429+1G>A) was identified in a 55-year-old man with multiple noradrenergic PGLs associated with bone metastasis,[16] and in one apparently unaffected relative with a positive biochemical diagnosis of the disease. Loss of heterozygosity (LOH) and significant reduction of MDH activity in the tumors suggested that *MDH2* acts as a tumor suppressor gene. As alterations in Krebs cycle genes have been associated with a higher metastatic risk of the disease, an early genetic diagnosis of unaffected carriers in these families seems to be crucial. However, that study did not address the contribution of *MDH2* to the global PPGL susceptibility or the clinical features associated with PV in this gene.

Correspondence: Mercedes Robledo (mrobledo@cnio.es). [#]A full list of authors and their affliations appears at the end of the paper.
These authors contributed equally: Bruna Calsina and Maria Currás-Freixes

Submitted 13 September 2017; accepted: 7 May 2018
Published online: 16 July 2018

Table 1 Clinical characteristics of the patients included in the study

	NUMBER (percentage)				
PATIENTS	830				
DNA germline	641 (77.2%)	Total DNA samples: 849			
DNA tumor	170 (20.5%)				
DNA matched tumor-germline	19 (2.3%)				
SEX					
Female	449 (57.8%)				
Male	328 (42.2%)				
No data	53				
AGE AT PRESENTATION					
Median (IQR)	39 (29-56) years				
Younger than 35	334 (40.2 %)				
FAMILIAL PPGL	13 (1.7%)				
LOCATION					
SINGLE	678 (85.2%)	**MULTIPLE**	118 (14.8%)	**No data**	34
PCC	427	PCC	32		
HN-PGL	146	HN-PGL	27		
A-PGL	83	A-PGL	18		
T-PGL	12	T-PGL	1		
No data	10	A- and T-PGL	4		
		A- and HN-PGL	6		
		HN- and T-PGL	1		
		PCC and A-PGL	22		
		PCC and T-PGL	4		
		PCC and HN-PGL	1		
		No data	2		
METASTASIS					
No	756 (91.1%)				
Yes	74 (8.9%)				
PREDOMINANTLY BIOCHEMICAL SECRETION					
Adrenergic	60	No secretion	176		
Noradrenergic	237	High, but unspecified	132		
Dopaminergic	4	No data	221		

IQR interquartile range, *PCC* pheochromocytoma, *PGL* paraganglioma, *HN* head and neck, *A* abdominal, *T* thoracic, *PPGL* pheochromocytoma/paraganglioma

One of the main challenges for genetic screening is the classification of variants of unknown significance (VUS) to improve genetic counseling and clinical follow-up of PV carriers. The pathogenicity assessment of VUS requires taking into account the frequency reported in several databases, in silico effect prediction and functional assays.

In this international collaborative study, we determined the prevalence of germline and/or somatic *MDH2* PV, and the associated phenotype in 830 unrelated PPGL index patients, negative for at least the main 13 driver PPGL susceptibility genes. Secondly, we developed a workflow of in silico predictions and simulations, and functional studies for assessing the functional impact of *MDH2* VUS identified.

All *MDH2* genetic changes, except one in-frame deletion and one variant affecting a donor splice-site, consisted of single-nucleotide substitutions leading to missense, synonymous, or intronic changes, for which we assessed their functional impact. Those MDH2 VUS were analyzed with one of five approaches: (1) applying 20 computational methods to predict their effect at the level of protein structure and function, implementing an enzymatic assay to assess : (2) MDH2 activity and (3) MDH2 affinity; (4) designing an immunofluorescence assay to evaluate MDH2 localization changes; and (5) using a molecular dynamics (MD) simulation approach to examine the potential changes in protein structure and dynamics for the most controversial variants. This sequential scheme aimed to categorize the vast majority of *MDH2* VUS found in an extensive setting.

MATERIALS AND METHODS

Patients

Diagnosis of PPGL was established following conventional methods (including clinical, biochemical, imaging, and pathological data). A new series of 561 PPGL index cases negative for at least 13 major PPGL genes (*RET, VHL*, SDH genes, *NF1*, *HRAS*, *EPAS1*, *MAX*, *TMEM127*, and *FH*) and not previously tested for *MDH2* were screened by Sanger (SS) or a next-generation (NGS) sequencing panel (PheoSeq[17]). To establish the prevalence of *MDH2* PV and classify *MDH2* VUS, we also considered 269 previously reported patients with negative genetic screening for the 13 PPGL genes, but including 4 carriers of *MDH2* VUS.[17] This outstanding series of 830 unrelated PPGL index patients was recruited through a collaborative effort from 11 participating centers: 10 of the European Network for the Study of Adrenal Tumors (ENS@T) consortium (Madrid, Paris, Liège, Würzburg, Munich, Dresden, Florence, Rotterdam, Delft, and Nijmegen), and one in the United States (Bethesda).

Clinical data were collected as previously described.[18] Table 1 summarizes the clinical characteristics of patients, who provided informed consent to collect clinical and genetic data, in accordance with institutional ethical–approved protocols for each center. In addition, tumor tissues from the Erasmus MC (Rotterdam, The Netherlands) and the Radboud University Medical Centre (Nijmegen, The Netherlands) were used according to the code of conduct: "Proper Secondary Use of Human Tissue" established by the Dutch Federation of Medical Scientific Societies.

Samples

A total of 849 DNA samples from the 830 patients were available for this study. DNA was obtained exclusively from blood in 641 patients, tumor in 170 patients, and matched tumor-blood in 19 patients (Table 1). Tumor samples were formalin-fixed paraffin-embedded (FFPE) tissues in 80 (42.3%) and frozen tissues in 109 (57.7%) of the cases.

Germline DNA was extracted from peripheral blood samples following a standard method (FlexiGene DNA Kit, Qiagen). DNeasy Blood & Tissue Kit (Qiagen) and truXTRAC FFPE DNA microTUBE Kit (Covaris, MA, USA) were used to extract DNA from frozen tumor tissue and from FFPE tumor samples, respectively, following the manufacturer's instructions.

Molecular genetic analyses

MDH2 genetic screening was performed in the CNIO (Madrid) and in the HEGP (Paris), either by NGS panel or SS. Primers sequences spanning the nine exons and intron–exon boundaries of *MDH2* were those previously described.[16]

MDH2 gross deletions were tested in 216 cases with good germline DNA quality using a semiquantitative multiplex polymerase chain reaction (PCR) method with labeled primers, as previously described for other genes.[16,19]

The variant calling was based on the *MDH2* transcript ENST00000315758.9. The frequency of *MDH2* variants was investigated in public databases: dbSNP (https://www.ncbi.nlm.nih.gov/SNP), COSMIC (http://cancer.sanger.ac.uk/cosmic), and gnomAD (http://gnomad.broadinstitute.org/).

MDH2 variants identified in <0.1% of the population and without homozygotes described were included in the study and used for further analyses. LOH of the *MDH2* variants in tumor DNA was assessed by direct sequencing (if material was available).

MDH2 expression by immunohistochemistry

Immunohistochemistry was performed as described in Supplemental Methods.

Computational prediction of functional impact

Three distinct in silico approaches were used to assess the functional and three-dimensional (3D) structural effect of the missense variants: (1) measure of the evolutionary conservation in the genome of vertebrate and mammalian species (i.e., phyloP, phastCons, GERP++), (2) prediction of the impact of amino acid substitutions in protein function (i.e., SIFT, Polyphen2, LRT, MutationAssessor, fathmm-MKL, PROVEAN, MetaSVM, MetaLR, MutationTaster), and (3) prediction of protein 3D destabilization (i.e., PoPMuSiCv3.1, CUPSAT, I-Mutant v3.0, MAESTRO, INPS-3D).

A consensus interpretation was established according to the number of tools predicting a damaging effect versus a benign

or tolerated one. The consensus was given if at least 70% (functional impact: 7 of 10; 3D stability: 4 of 5) of the predictors agreed in the variant classification. Otherwise, the results were considered as inconclusive.

Moreover, we included functional annotations (e.g., ligand binding sites, catalytic residues, posttranslational modifications of proteins, residues in protein–protein interaction interfaces) retrieved by the Structure-PPi system.[20] Structure-PPi also considers residues in physical proximity (at a distance of 5 Å) to amino acid changes found in other type of cancers.

ESEFinder and RESCUE-ESE using Alamut Visual software version 2.7 (Interactive Biosoftware, Rouen, France) were used to predict splicing changes in synonymous and intronic variants.

RBP1 gene expression analysis

The low expression of retinol binding protein 1 (*RBP1*) is a marker of Krebs cycle disruption.[21] Its assessment is detailed in Supplemental Methods.

Plasmids and cell culture

QuickChange Lightning Site-Directed Mutagenesis Kit (Agilent) was used to generate missense variants in pCMV6-AC-MDH2 (Origene), a plasmid containing the full complementary DNA (cDNA) sequence (NM_005918) of the human *MDH2* gene. We generated a polymorphism with a minor allele frequency (MAF) = 0.037 in gnomAD (rs10256: p.Lys301Arg), to be used as control. Primers used to generate mutated vectors are described in Table S1. The introduction of the PV of interest was confirmed by SS (Fig. S1).

Sh8561 *MDH2* knockdown Hela cells[16] (*MDH2* KD cells) culture conditions are specified in Supplemental Methods.

Microscopic analysis

For immunofluorescence imaging, 300,000 cells were seeded 24 h before transfection on coverslips in 12-well plates. Cells were transiently transfected with 2 µg of plasmids mutated with each variant using Lipofectamine 2000 (Invitrogen) following the vendor's manual. Twenty-four hours after transfection cells were stained as described in Supplemental Methods and analyzed by confocal microscopy (Leica TCS SP5 X).

In silico molecular dynamics (MD) simulations

The initial model of the system used the crystal structure of a tetramer of oxaloacetate and NADH-bound MDH2 (PDBid: 4wlo). The structure contains coordinates for residues 24–337 of each monomer. The dimer formed by monomers A and B was extracted and ligands and crystal waters were removed. Missing hydrogen atoms were added using the H++server,[22] and in the case of the mutants, the point variants were introduced using Pymol.[23] The systems were placed in dodecahedral boxes, with the minimal distance between the protein and the borders of the box being 10 Å. The systems were solvated with TIP3P waters,[24] and Na^+/CL^- was added to neutralize them to obtain a physiological salt concentration of 0.15 mol/l. First, the systems were minimized during 500 steps, applying the steepest descent algorithm. Consequently, the solvent was equilibrated for 100 ps in the NVT ensemble, followed by another 100 ps in the isobaric–isothermal (NpT) ensemble. The resulting configurations were used for MD production runs of 400 ns for each system. The trajectories were analyzed by principal component analysis (PCA) (see Supplemental Methods).

Simulations and analyses of the trajectories were performed as described in Supplemental Methods[25–31].

Enzymatic activity assay

MDH2 KD cells were seeded in T150 flasks at $16{\cdot}10^6$ cells/flask 24 h before transfection. Each flask was transiently transfected with 20 µg of each variant plasmid using Lipofectamine 2000 (Invitrogen), according to the manufacturer's recommendations. *MDH2* KD cells transfected either with wild-type (WT) cDNA (pCMV6-AC-*MDH2*), *MDH2* KD cells with pCMV6-AC empty vector (EV), or *MDH2* KD cells with pCMV6-AC-*MDH2*-c.902A>G vector were used as controls. To mimic the heterozygous state of p.Arg104Gly patient, we cotransfected 10 µg pCMV6-AC-*MDH2* and 10 µg pCMV6-AC-*MDH2*-c.310A>G plasmids; as control, we used cells cotransfected with 10 µg pCMV6-AC-*MDH2* and 10 µg pCMV6-AC EV, and 20 µg EV alone. Twenty-four hours after transfection, enzymatic activity assay was performed as described in Supplemental Methods.

RESULTS

MDH2 variants and computational analyses

Twelve *MDH2* heterozygous variants (Fig. 1) were found, demonstrating a germline origin for 11 of them (only tumor DNA was available in the remaining case). Clinical data of the *MDH2* carriers are detailed in Table S3. None of the patients had family history of the disease.

Five of the 12 were missense (41.7%), 1 synonymous (8.3%), 4 were located in the intronic region (33.3%), 1 was an in-frame deletion (8.3%), and 1 affected a donor splice-site (8.3%) (Fig. 1). Five of them were unreported variants (3 missense, 1 intronic, and 1 in-frame deletion), six showed a low allele frequency ($<1{\cdot}10^{-3}$) and no homozygotes in gnomAD, and the donor splice-site variant had been previously suggested to be pathogenic[16] (Table 2; Table S5). The two probands with the splice-site *MDH2* PV are not related.

The synonymous variant (p.Phe333Phe), found in a patient with a nonfunctional T-PGL, had no effect according to in silico splicing predictors (Table S5). Similarly, the splicing for three of the four intronic variants (c.320-26A>C, c.733 +47G>A, and c.734- 5C>A) was not predicted affected, while it was anticipated as altered in the remaining intronic variant (c.319+37G>A) identified in a 48-year-old patient with a noradrenergic PCC. RNA of this patient was not available to confirm this prediction.

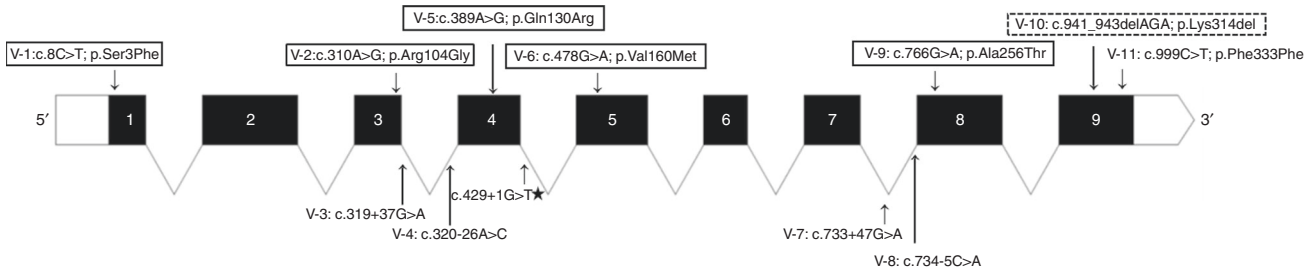

Fig. 1 Graphical representation of the variants identified in *MDH2* and the residues of the protein affected. The PV previously reported[16] is indicated with a star. Missense variants are framed in continuous line; in-frame deletion is framed in discontinuous line; synonymous variant is shown in the upper part of the figure; intronic variants are shown in the lower part of the figure

Of the five *MDH2* missense variants identified (Table 2), only one (p.Ser3Phe) was outside the functional domains in the transit peptide to mitochondria. The variants p.Arg104Gly, p.Gln130Arg, and p.Val160Met were positioned in the lactate/malate dehydrogenase, NAD-binding domain; and p.Ala256Thr in the lactate/malate dehydrogenase, alpha/beta C-terminal domain. Furthermore, they affected conserved positions in vertebrate and mammalian species, as indicated by phyloP, phastCons, and GERP++ methods. Indeed, p.Arg104Gly is positioned in the NAD-binding site.

Three of the missense variants (p.Arg104Gly, p.Val160Met, and p.Ala256Thr) were predicted to have a damaging effect (*impaired* functional predictions and *destabilization* of the 3D structure) (Table 2; Table S4). The variant p.Ser3Phe was classified as *inconclusive* according to the functional impact predictions and the corresponding 3D structural predictions could not be performed (residue not present in the crystal structure [PDB ID: 2DFD]). The variant p.Gln130Arg was categorized as *neutral* and *inconclusive* according to the functional and 3D structure predictions, respectively. Moreover, the COSMIC database reported *MDH2* somatic PV in other cancers in neighbor positions ($d \leq 5$ Å), as indicated by Structure-PPi (Fig. S2), for all the variants except for p.Ser3Phe.

The variants p.Arg104Gly and p.Ala256Thr were found in two young patients (25 and 29 years old, respectively) with norepinephrine-producing PCC both diagnosed during pregnancy. One of them developed metachronous bone metastases. The p.Val160Met was identified in a PCC patient without biochemical data. The remaining two missense variants (p.Ser3Phe and p.Gln130Arg) were found in patients older than 45 years, diagnosed with PCC; the former involving an adrenergic tumor and the latter without evidence of excess in catecholamine production (Table S3).

A previously unreported in-frame deletion (p.Lys314del) was found in a 55-year-old patient, with multiple noradrenergic PGLs. It affected a conserved residue, for which PV in neighboring residues have been described in several cancers (Table 2; Fig. S2); LOH was demonstrated in the tumor.

Furthermore, the c.429+1G>T variant, previously described,[16] was found in a 57-year-old patient diagnosed with a PCC and liver metastases.

MDH2 immunohistochemistry

MDH2 immunohistochemistry it is not useful to classify VUS or select patients for *MDH2* screening (see Supplemental Results).

RBP1 expression in *MDH2* variants

RBP1 measurement was performed in four available tumors (p.Ser3Phe, p.Arg104Gly, p.Val160Met, and p.Lys314del–tumor), observing a reduced *RBP1* expression in three tumors compared with controls: 93.86 ± 1.83% ($p = 0.007$), 83.18 ± 0.65% ($p = 0.007$), and 82.44 ± 19.72% ($p = 0.030$) for p.Lys314del-, p.Arg104Gly-, and p.Val160Met-tumor, respectively (Fig. S3).

MDH2 localization

None of the variants was associated with an altered MDH2 localization, or mitochondrial quantity and morphology (see Supplemental Results).

Enzymatic activity characterization

Only variant p.Arg104Gly displayed a significant lower MDH2 enzymatic activity at saturating concentration of substrates ($p < 0.0001$) compared with WT, comparable with the activity detected in the KD cells not expressing MDH2 (Fig. 2a). On the other hand, citrate synthase activity, present exclusively in the mitochondria, was similar for all variants (Table S2), suggesting that none of them produced an increased mitochondrial biogenesis to compensate the possible aberrant *MDH2* variant. Thus, this functional assay only supported pathogenicity for p.Arg104Gly, having an incomplete functional proof of in silico predictions.

Enzymatic activity assay to check a dominant-negative effect

LOH was not detected in any of the tumors carrying the missense variants. To evaluate if *MDH2* variants could exert a dominant-negative effect on MDH2 WT, we took as a model the p.Arg104Gly variant. We cotransfected WT plasmid, p.Arg104Gly plasmid, and a combination of both to mimic the heterozygous state of the mutated patient. EV was used to achieve the same amount of total transfected plasmid (20 µg in each cotransfection). Cells cotransfected with both WT and p.Arg104Gly plasmids exhibited lower enzymatic

Table 2 Summary of the in silico and in vitro analyses in *MDH2* missense and deletion VUS

VUS		V-1 p.Ser3Phe	V-2 p.Arg104Gly	V-5 p.Gln130Arg	V-6 p.Val160Met	V-9 p.Ala256Thr	V-10 p.Lys314del
SNP ID ExAC allele freq. gnomAD* allele freq. 1000 Genomes*		not described	not described	not described	rs138541865 $1{,}66{\cdot}10^{-4}$; 0 hom -	rs147655350 $4{,}69{\cdot}10^{-5}$; 0 hom -	not described
Evolutionary conservation ***Interpretation*** (a)		Conserved position	Conserved position	Conserved position	Conserved position	Conserved position	Conserved position ¤
Functional domain		NA (Low complexity region)	Ldh_1_N domain (PF00056)	Ldh_1_N domain (PF00056)	Ldh_1_N domain (PF00056)	Ldh_1_C domain (PF02866)	Ldh_1_C domain (PF02866)
Protein function prediction ***Interpretation*** (a)		Inconclusive (5/9)	**Impaired (10/10)**	Neutral (3/10)	**Impaired (8/10)**	**Impaired (9/10)**	NA
3D structural annotations (Structure-PPi)		Transit peptide to Mitochondria (aa 1-24)	NAD-binding site	α-helix	NA	α-helix	α-helix
3D structural prediction ***Interpretation*** (a)		No effect	**Destabilize (4/5)**	Inconclusive (3/5)	**Destabilize (5/5)**	**Destabilize (5/5)**	NA
Neighbor positions mutated in other cancers (b) (Structure-PPi)		NA	Malignant melanoma, Ovary carcinoma, Colon carcinoma, Endometrium carcinoma	Breast carcinoma	Stomach carcinoma	Endometrium carcinoma, Head and neck squamous cell carcinoma	Endometrioid Carcinoma (p.Ser310Ser), Prostate carcinoma (p.Ser317Leu), Oral carcinoma (p.Ala319Ser)
***RBP1* expression** (c)		+++	+	NA	+	NA	+
LOH		no	no	NA	no	NA	**Yes**
MDH2 subcelular localization (d)		M	M	M	M	M	NA
Enzymatic activity	**with saturating [NAD+] and [malate]** (e)	+++	+	+++	+++	+++	NA
	co-transfection experiment (e)	NA	++	NA	NA	NA	NA
	Affinity assay: with lower [NAD+] and [malate] (f)	NA	**Impaired for malate and NAD^+**	NA	**Likely impaired for malate**	**Likely impaired for malate and NAD+**	NA
Molecular dynamics simulations		NA	NA	NA	**Substrate binding site likely affected**	**Dimerization likely affected**	NA
Classification of VUS		**LIKELY BENIGN**	**PATHOGENIC**	**LIKELY BENIGN**	**LIKELY PATHOGENIC**	**LIKELY PATHOGENIC**	**PATHOGENIC**

Results in bold indicate major alterations. *V-* variant, *NA* not available, *Ldh_1_N domain* lactate/malate dehydrogenase, NAD-binding domain (Pfam accession: PF00056), *Ldh_1_C domain* lactate/malate dehydrogenase, alpha/beta C-terminal domain (Pfam accession: PF02866), *SNP* single-nucleotide polymorphism, *VUS* variant of unknown significance, *M* mitochondrial

[a]See Table S4 for breakdown of the different computational predictors. The number of tools predicting a damaging effect is in brackets

[b]See Fig. S2 for mapping of the pathogenic variant onto the crystal structure

[c]*RBP1* messenger RNA (mRNA) expression relative to tumors with pathogenic variants in non-Krebs cycle genes: +++ corresponds to nonsignificant *RBP1* expression reduction, + corresponds to significant ($p < 0.05$) *RBP1* expression reduction

[d] M: mitochondrial subcelular localization [e] From in vitro MDH2 enzymatic activity (Fig. **2a, b**): +++ corresponds to MDH2 activity >75% compared with control, ++ 25–75%, and + 0–25%

[e]f From in vitro MDH2 enzymatic affinity assay (Fig. **2c-f**)

*http://gnomad.broadinstitute.org/ and http://www.internationalgenome.org/ (Last accessed 7 June 2017)

[¤]Despite the fact that the variant p.K314del is not annotated in the dbNSFP database, we infer the evolutionary conservation of this position considering the annotated variants at this position (i.e., p.K314Q, p.K314E, p.K314*, p.K314T, p.K314R, p.K314M and p.K314N). For each method, the lowest and the highest scores are included

activity in comparison with those cotransfected with WT and EV ones (27.8% ± 22.6; $p = 0.0002$) (Fig. 2b).

MDH2 missense variants affinity characterization

Another assay was designed to evaluate if p.Val160Met and p.Ala256Thr variants affected the affinity of the enzyme for the substrates, instead of the maximal activity. We used the p.Arg104Gly variant as positive control. A tendency of reduced enzymatic activity when decreasing malate concentration was observed for p.Val160Met, significant at 5 mM (5-fold reduction to malate saturating concentration, $p = 0.0256$) (Fig. 2c) and at 2.5 mM (10-fold reduction to malate saturating concentration, $p = 0.0047$) (Fig. 2d). Furthermore, a subtle decrease in the activity was observed for p.Ala256Thr when diminishing concentration of NAD+ (Fig. 2f) and malate (Fig. 2d) to 20-fold ($p = 0.0464$) and 10-fold ($p = 0.0366$), respectively. No significant changes were observed at higher NAD+ concentrations (0.5 mM) (Fig. 2e).

Molecular dynamics (MD) simulations

Simulations of the dimers of the WT apoenzyme, and the p.Ala256Thr and p.Val160Met variants revealed differences in their principal motions. In the WT, we observed movements of the two monomers relative to each other, and large conformational changes in one of the helices of the substrate-binding site and its adjacent loop (Fig. S5A). In the p.Ala256Thr mutant, the character of the main motions was conserved (Fig. S5B), whereas in the p.Val160Met mutant the relative movement of the monomers was strongly reduced (Fig. S5C).

Although the dynamics of the p.Ala256Thr variant were similar to that of the WT, closer inspection revealed conformational changes. In the WT and p.Val160Met variant, the side chain of Phe260, neighboring Ala/Thr256, switches between two orientations, while in the p.Ala256Thr mutant it remains immobile (Fig. 3a). On a larger scale, the opening between the two monomers becomes slightly enlarged (Fig. 3b).

Even on a short time scale, the MD simulations revealed changes in conformation and dynamics of the variants, compared with the WT. The results suggest that the p.Ala256Thr variant affects the conformation of the neighboring residues, which contribute to the dimeric interface. This implies that the p.Ala256Thr variant may affect dimerization of MDH2. In the p.Val160Met variant, changes in the dynamics of the substrate-binding site may affect substrate affinity.

DISCUSSION

After the identification of major susceptibility PPGL genes, the list of other genes with modest contributions to the disease has kept growing and it is likely that this number will continue to increase over the near future.[3] Examples include *SDHA*,[32] *TMEM127*,[33] *MAX*,[34] or *FH*.[35] Through the use of NGS panels[36] to offer a comprehensive genetic diagnosis, multiple VUS are identified, for which the functional interpretation represents a crucial challenge in an accurate genetic counseling session. Herein, we aimed to determine the prevalence and the clinical characteristics of *MDH2* PV carriers in 830 patients with PPGL without PV in major PPGL susceptibility genes and to investigate the potential pathogenicity of every identified *MDH2* variant. We were able to classify 2 *MDH2* variants as pathogenic and provide evidence that suggests an altered molecular function of MDH2 in 2 others (which have been designated as likely PV), following the criteria established by the American College of Medical Genetics and Genomics and the Association for Molecular Pathology guidelines.[37] Furthermore, a new patient, carrying the already reported c.429+1G>T *MDH2* variant, was identified.

RBP1 expression in the tumor, bioinformatics predictions, and functional assays suggested that p.Arg104Gly is a PV located in the highly conserved NAD-binding site and significantly impairing MDH2 activity. This variant was found in a young patient with a noradrenergic PCC. PV in neighboring positions are reported in different cancers, supporting the implication of PV at this residue in the neoplastic process. However, neither LOH nor any other somatic PV was found in the corresponding tumor sample. Enzymatic assays performed by cotransfection of WT and p.Arg104Gly plasmids resembling the heterozygous character of this PV suggested a dominant-negative effect of the p.Arg104Gly-mutant.

The two other missense variants, p.Ala256Thr and p.Val160Met, reported as rare SNPs and located in conserved residues, were predicted to produce protein 3D structure destabilization and impaired the MDH2 molecular function. The p.Val160Met was detected in a 54-year-old PCC patient, whose tumor showed low *RBP1* expression. The p.Ala256Thr tumor sample was not available, so the interpretation of this variant was based exclusively on functional assays. This latter variant was found in a 29-year-old female with a noradrenergic metastatic PCC. The substitutions at residues Val160 and Ala256 could also affect the substrate binding affinity and protein 3D stability, and therefore, neither the enzymatic assay nor the immunofluorescence experiments are able to evaluate the effect. Because of that, we conducted MD simulations only with these variants, which suggested that p.Val160Met could be modifying malate binding to the catalytic site, and consequently affecting MDH2 affinity for its substrate. This was demonstrated in vitro, as MDH2 activity decreased when we reduced malate concentration, pointing to a lower affinity of the mutated enzyme for malate. For variant p.Ala256Thr, MD simulations predicted that it could be affecting enzyme dimerization. We observed a slight decrease in MDH2 activity when reducing both malate and NAD+ down to low concentrations, which could be related to impaired dimerization. A second somatic hit was not observed in the tumor of p.Val160Met-related patient and p.Ala256Thr-related tumor was not available. A dominant-negative effect for p.Val160Met and p.Ala256Thr variants might be the underlying mechanism as occurs with the p.

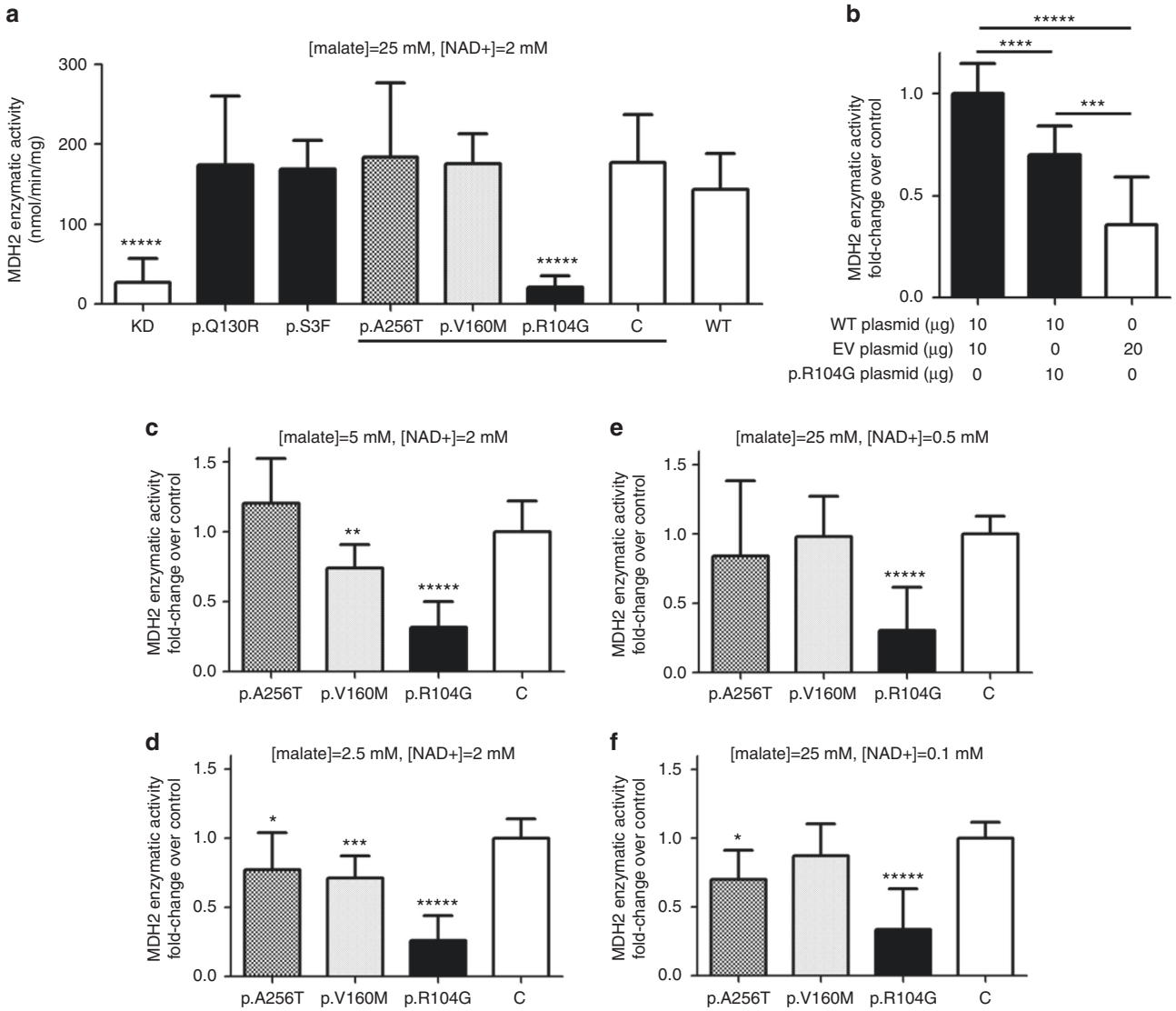

Fig. 2 MDH2 activity measured in *MDH2* KD cells transfected with different vectors containing the variant of unknown significance (VUS) in *MDH2*. **a** Enzymatic activities at saturating concentrations of malate (25 mM) and NAD+ (2 mM) in p.R104G (p.Arg104Gly), p.Q130R (p.Gln130Arg), p.V160M (p.Val160Met), and p.S3F (p.Ser3Phe) variants, plus C (p.K301R-p.Lys301Arg) which is a polymorphism with minor allele frequency of 0.037, knockdown (KD) and wild-type (WT) as controls, are expressed as mean (nmol/min/mg) ± SD of 3 paired independent experiments in quadruplicate. Different shadings indicate the only variants tested in experiments in **c**–**f**. **b** Enzymatic activities at saturating concentrations of cells cotransfected with WT, empty vector (EV), and/or p.R104G plasmids expressed as mean of fold-change over activity in cells cotransfected with WT and EV (control) ± SD of 2 paired independent experiments at least in quadruplicate; μg of plasmid DNA transfected for each condition are showed in the figure. **c–f** Enzymatic activities in p.A256T, p.V160M, p.R104G, and control (p.K301R) expressed as mean of fold-change over control ± SD of at least 2 paired independent experiments in triplicate. Assays performed with reduced concentrations of malate or NAD+: **c** 5-fold reduction malate (5 mM), **d** 10-fold reduction malate (2.5 mM), **e** 4-fold reduction of NAD+ (0.5 mM), and **f** 20-fold reduction of NAD+ (0.1 mM). *****$p < 0.0001$, ****$p < 0.001$, ***$p < 0.01$, **$p < 0.03$, and *$p < 0.05$ based on a two-sided Mann–Whitney *U* test

Arg104Gly variant, although this has not been tested in this study. Thus, the p.Ala256Thr variant could be classified as likely pathogenic. Regarding the p.Val160Met variant, although most of our analyses suggested a potential pathogenic role as well, it was also classified as likely pathogenic due to the high number of alleles found (46/277206) in the general population.

For the two other novel missense variants (p.Ser3Phe and p.Gln130Arg) identified, computational analyses did not reach a consensus. In addition, patients carrying these variants had predominant adrenaline production or nonfunctional tumors, which is in discordance with *MDH2*-mutated patient[16] and other Krebs cycle genes. The high *RBP1* expression in the p.Ser3Phe-tumor supported that this variant is not pathogenic. Thus, we classified these two variants as likely neutral.

The four intronic variants and the synonymous one were not classified, as no RNA was available. The computational

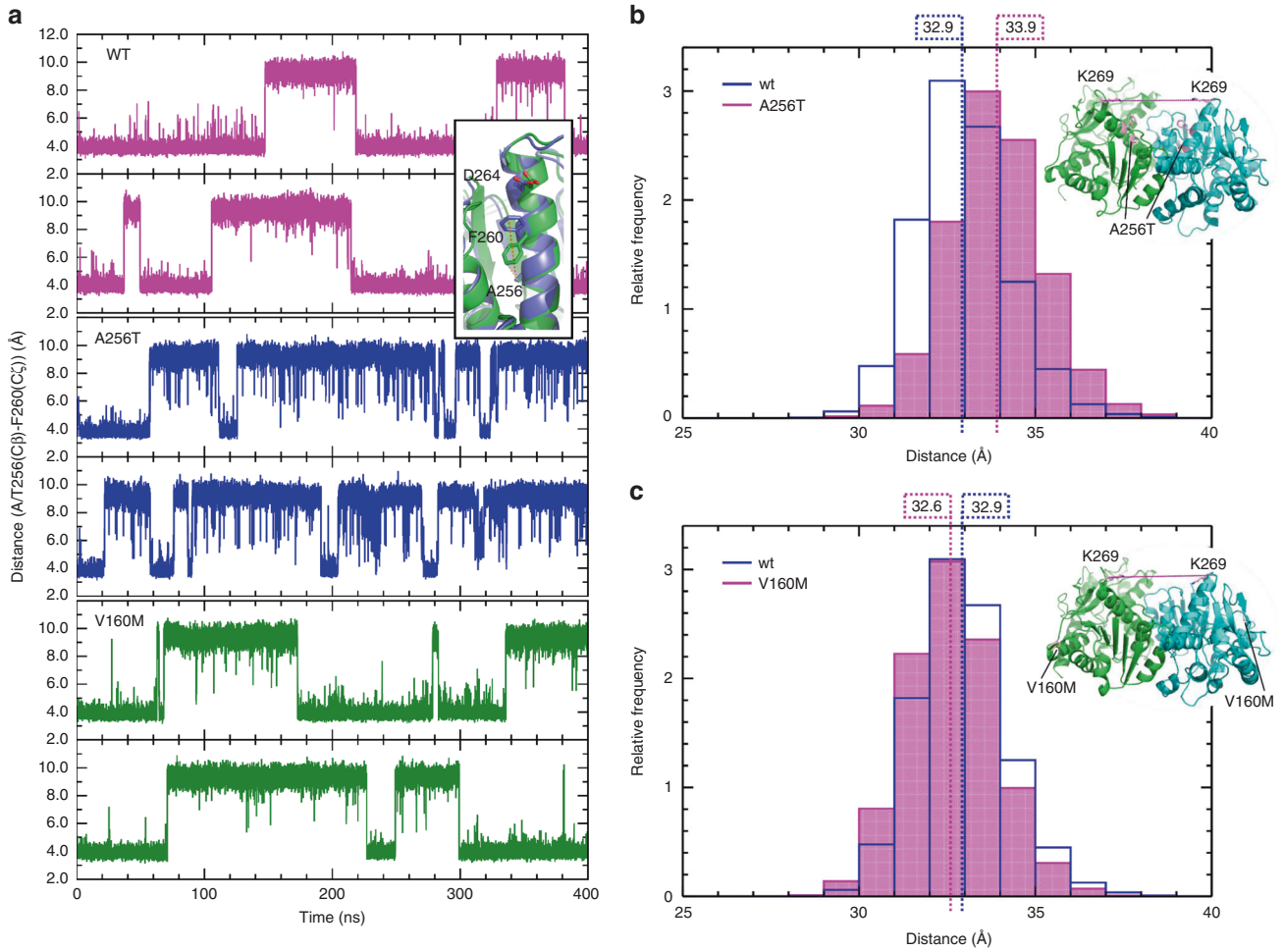

Fig. 3 Molecular dynamics simulations in MDH2 p.Ala256Thr and p.Val160Met variants of unknown significance (VUS) versus wild-type (WT). **a** Distance between the Cζ atom of F260 and the Cβ atom of A/T256 for both monomers of WT MDH2 (magenta, upper panels), Ala256Thr (blue, middle panels), and V160M (green, lower panels) during the simulations. A short distance corresponds to the F260 down conformation, and a long distance to the F260 up conformation (inset). **b** and **c** Distribution of the distance between the Cα atoms of K269 of the two monomers of the **a** Ala256Thr and **b** Val160Met variants from snapshots from the simulation trajectories, compared with WT

tools indicated no agreement, highlighting the relevance of having access to a tissue tumor sample to study at least the *RBP1* and/or *MDH2* expression.

The p.Lys314del, identified in a patient with multiple noradrenergic PGLs, was classified as pathogenic, as it affects a conserved amino acid, and LOH and low *RBP1* expression in the tumor sample were found.

Finally, a 57-year-old patient with a metastatic pheochromocytoma, clinical phenotype similar to the patient reported,[16] was identified to carry the same variant affecting a donor splice-site (c.429+1G>A).

In summary, taking into account only those *MDH2* variants identified that display characteristics supportive of a pathogenicity potential, we provide more evidence that suggests the potential role of *MDH2* in PPGL predisposition, and indicates that *MDH2* germline PV could be responsible for 0.6% of PPGL cases, prevalence comparable with that reported for other recently described PPGL genes. The apparent lack of family history in four pedigrees investigated suggests an incomplete penetrance of *MDH2*, similar to the one observed in other Krebs cycle genes, such as *SDHA* or *FH*. Furthermore, there are other similarities worthy to mention. In this regard, families affected with encephalopathy due to recessive MDH2 deficiency have been described.[38] One could expect to find PPGL patients in these families, but as it happens in pedigrees affected with the Leigh syndrome (OMIM 256000) associated with autosomal recessive PV in *SDHA*,[39] their members do not develop either these tumors.

On the other hand, it is worthy to note that *MDH2* variants were found in metastatic cases, as two of five patients (three of six, if we include the reported *MDH2* patient)[16] developed metastases. Taking into account the low prevalence of *MDH2* PV, as well as the low penetrance, its genetic testing could be considered in a research direction manner until providing further epidemiological and segregation data that would confirm the implication of *MDH2* PV in PPGL susceptibility.

NGS is becoming the rational tool to apply to PPGL genetic diagnosis, and unavoidably it leads to an increasing number of

VUS reported. The task of classifying VUS for genetic counseling is especially complex when considering genes scarcely analyzed, which exhibit a high ratio of missense variants, as previously shown for *MAX*.[40] In this study, we were able to demonstrate a functional impact for two variants (p.Arg104Gly and p.Lys314del) and suggested an altered molecular function for other two (p.Val160Met and p.Ala256Thr), but there was insufficient evidence to consider them pathogenic even after applying up to five approaches to classify them. Although, it is likely that this rationale is unapproachable in the clinical setting when tumor tissue is unavailable, we demonstrated that *MDH2* variants could be classified by a multidisciplinary approach.

ELECTRONIC SUPPLEMENTARY MATERIAL

The online version of this article (https://doi.org/10.1038/s41436-018-0068-7) contains supplementary material, which is available to authorized users.

ACKNOWLEDGEMENTS

We gratefully acknowledge Diego Megias and all Confocal Microscopy Core Unit (CNIO) team for their technical support and advice, as well as Santiago Ramón-Maiques from Structural Bases of Genome Integrity Group (CNIO) for fruitful discussions. This work was supported by the Instituto de Salud Carlos III (ISCIII), Acción Estratégica en Salud, (projects PI14/00240 and PI17/01796), cofinanced by Fondo Europeo de Desarrollo Regional (FEDER), GETNE (Grupo Español de Tumores Neuroendocrinos), the European Union Seventh Framework Programme (FP7/2007-2013) under grant agreement no. 259735, the Paradifference foundation, and the Intramural Research Program of the National Institutes of Health (NIH) and National Institute of Child Health and Human Development (NICHD). Bruna Calsina is supported by the Becas de excelencia Rafael del Pino 2017, Maria Currás-Freixes was supported by the Severo Ochoa Excellence Programme (project SEV-2011-0191), Laura Contreras by a CIBERER contract, Alexandre Buffet received financial support from ITMO Cancer AVIESAN (Alliance Nationale pour les Sciences de la Vie et de la Santé, National Alliance for Life Sciences & Health) within the framework of the Cancer Plan, and Susan Richter is supported by the Deutsche Forschungsgemeinschaft (RI 2684/1-1).

DISCLOSURE

The authors declare no conflicts of interest.

REFERENCES

1. Dahia PLM. Pheochromocytoma and paraganglioma pathogenesis: learning from genetic heterogeneity. *Nat Rev Cancer*. 2014;14:108–19.
2. Crona J, Backman S, Maharjan R, et al. Spatiotemporal heterogeneity characterizes the genetic landscape of pheochromocytoma and defines early events in tumorigenesis. *Clin Cancer Res*. 2015;21:4451–4460.
3. Favier J, Amar L, Gimenez-Roqueplo A-P. Paraganglioma and phaeochromocytoma: from genetics to personalized medicine. *Nat Rev Endocrinol*. 2014;11:101–11.
4. Gaal J, Burnichon N, Korpershoek E, et al. Isocitrate dehydrogenase mutations are rare in pheochromocytomas and paragangliomas. *J Clin Endocrinol Metab*. 2010;95:1274–1278.
5. Yang C, Zhuang Z, Fliedner SMJ, et al. Germ-line PHD1 and PHD2 mutations detected in patients with pheochromocytoma/paraganglioma-polycythemia. *J Mol Med*. 2014;93:93–104.
6. Fishbein L, Khare S, Wubbenhorst B, et al. Whole-exome sequencing identifies somatic ATRX mutations in pheochromocytomas and paragangliomas. *Nat Commun*. 2015;6:6140.
7. Castro-Vega LJ, Letouze E, Burnichon N, et al. Multi-omics analysis defines core genomic alterations in pheochromocytomas and paragangliomas. *Nat Commun*. 2015;6:6044.
8. Luchetti A, Walsh D, Rodger F, et al. Profiling of somatic mutations in phaeochromocytoma and paraganglioma by targeted next generation sequencing analysis. *Int J Endocrinol*. 2015;2015:138573.
9. Toledo RA, Qin Y, Cheng ZM, et al. Recurrent Mutations of Chromatin-Remodeling Genes and Kinase Receptors in Pheochromocytomas and Paragangliomas. *Clin Cancer Res*. 2016;22:2301–2310
10. Castro-Vega LJ, Kiando SR, Burnichon N, Buffet A, Amar L, Simian C. The MITF, p.E318K variant as a risk factor for pheochromocytoma and paraganglioma. *J Clin Endocrinol Metab*. 2016;101:4764–4768.
11. Fishbein L, Leshchiner I, Walter V, et al. Comprehensive molecular characterization of pheochromocytoma and paraganglioma. *Cancer Cell*. 2017;31:181–193.
12. Remacha L, Comino-Méndez I, Richter S, et al. Targeted Exome Sequencing of Krebs Cycle Genes Reveals Candidate Cancer–Predisposing Mutations in Pheochromocytomas and Paragangliomas. *Clin Cancer Res*. 2017;23:6315–6324.
13. Papathomas TG, Oudijk L, Zwarthoff EC, et al. Telomerase reverse transcriptase promoter mutations in tumors originating from the adrenal gland and extra-adrenal paraganglia. *Endocr Relat Cancer*. 2014;21:653–661.
14. Liu T, Brown TC, Juhlin CC, et al. The activating TERT promoter mutation C228T is recurrent in subsets of adrenal tumors. *Endocr Relat Cancer*. 2014;21:427–434.
15. Richter S, Klink B, Nacke B, et al. Epigenetic mutation of the succinate dehydrogenase C promoter in a patient with two paragangliomas. *J Clin Endocrinol Metab*. 2016;101:359–363.
16. Cascón A, Comino-Méndez I, Currás-Freixes M, et al. Whole-exome sequencing identifies MDH2 as a new familial paraganglioma gene. *J Natl Cancer Inst*. 2015;107:1–5.
17. Currás-Freixes M, Piñeiro-Yañez E, Montero-Conde C, et al. PheoSeq: a targeted next-generation sequencing assay for pheochromocytoma and paraganglioma diagnostics. *J Mol Diagn*.2017;19:575–588
18. Currás-Freixes M, Inglada-Pérez L, Mancikova V, et al. Recommendations for somatic and germline genetic testing of single pheochromocytoma and paraganglioma based on findings from a series of 329 patients. *J Med Genet*. 2015;52:647–656.
19. Cascón A, Montero-Conde C, Ruiz-Llorente S, et al. Gross SDHB deletions in patients with paraganglioma detected by multiplex PCR: a possible hot spot? *Genes Chromosomes Cancer*. 2006;45:213–219.
20. Vázquez M, Valencia A, Pons T. Structure-PPi: a module for the annotation of cancer-related single-nucleotide variants at protein-protein interfaces. *Bioinformatics*. 2015;31:2397–2399.
21. Chou AP, Chowdhury R, Li S, et al. Identification of retinol binding protein 1 promoter hypermethylation in isocitrate dehydrogenase 1 and 2 mutant gliomas. *J Natl Cancer Inst*. 2012;104:1458–1469.
22. Gordon JC, Myers JB, Folta T, et al. H++: a server for estimating pKas and adding missing hydrogens to macromolecules. *Nucleic Acids Res*. 2005;33:W368–71.
23. DeLano WL. The PyMOL molecular graphics system. Schrödinger LLC. Version 1. 2002. http://www.pymol.org. needs an acces date.
24. Mahoney MW, Jorgensen WL. A five-site model for liquid water and the reproduction of the density anomaly by rigid, nonpolarizable potential functions. *J Chem Phys*. 2000;112:8910.
25. Van Der Spoel D, Lindahl E, Hess B et al. GROMACS: fast, flexible, and free. *J Comput Chem*. 2005;26:1701–1718.
26. Hess B, Kutzner C, Van Der Spoel D, Lindahl E. GRGMACS 4: algorithms for highly efficient, load-balanced, and scalable molecular simulation. *J Chem Theory Comput*. 2008;4:435–447.
27. Abraham MJ, Murtola T, Schulz R et al. Gromacs: high performance molecular simulations through multi-level parallelism from laptops to supercomputers. *SoftwareX*. 2015;1–2:19–25.
28. Lindorff-Larsen K, Piana S, Palmo K et al. Improved side-chain torsion potentials for the Amber ff99SB protein force field. *Proteins*. 2010;78:1950–1958.

29. Best RB, Hummer G. Optimized molecular dynamics force fields applied to the helix-coil transition of polypeptides. *J Phys Chem B*. 2009;113: 9004–9015.
30. Bussi G, Donadio D, Parrinello M. Canonical sampling through velocity rescaling. *J Chem Phys*. 2007;126:014101.
31. Parrinello M, Rahman A. Polymorphic transitions in single crystals: a new molecular dynamics method. *J Appl Phys*. 1981;52:7182–7190.
32. Korpershoek E, Favier J, Gaal J, et al. SDHA immunohistochemistry detects germline SDHA gene mutations in apparently sporadic paragangliomas and pheochromocytomas. *J Clin Endocrinol Metab*.2011;96:E1472–1476
33. Qin Y, Yao L, King EE, et al. Germline mutations in TMEM127 confer susceptibility to pheochromocytoma. *Nat Genet*. 2010;42:229–233.
34. Comino-Méndez I, Gracia-Aznárez FJ, Schiavi F, et al. Exome sequencing identifies MAX mutations as a cause of hereditary pheochromocytoma. *Nat Genet*. 2011;43:663–667.
35. Castro-Vega LJ, Buffet A, De Cubas AA, et al. Germline mutations in FH confer predisposition to malignant pheochromocytomas and paragangliomas. *Hum Mol Genet*. 2014;23:2440–2446.
36. Toledo RA, Burnichon N, Cascon A, et al. Consensus statement on next-generation-sequencing-based diagnostic testing of hereditary phaeochromocytomas and paragangliomas. *Nat Rev Endocrinol*. 2016;13:233–247.
37. Richards S, Aziz N, Bale S, et al. Standards and guidelines for the interpretation of sequence variants: a joint consensus recommendation of the American College of Medical Genetics and Genomics and the Association for Molecular Pathology. *Genet Med*. 2015;17:405–424.
38. Ait-El-Mkadem S, Dayem-Quere M, Gusic M, et al. Mutations in MDH2, encoding a Krebs cycle enzyme, cause early-onset severe encephalopathy. *Am J Hum Genet*. 2017;100:151–159.
39. Renkema GH, Wortmann SB, Smeets RJ, et al. SDHA mutations causing a multisystem mitochondrial disease: novel mutations and genetic overlap with hereditary tumors. *Eur J Hum Genet*. 2015;23:202–209.
40. Comino-Méndez I, Leandro-García LJ, Montoya G, et al. Functional and in silico assessment of MAX variants of unknown significance. *J Mol Med*. 2015;93:1247–1255.

Bruna Calsina, MSc[1], Maria Currás-Freixes, MD, PhD[1], Alexandre Buffet, MSc[2], Tirso Pons, PhD[3,4], Laura Contreras, PhD[5,6], Rocío Letón, BSc[1], Iñaki Comino-Méndez, PhD[1], Laura Remacha, MSc[1], María Calatayud, MD[7], Berta Obispo, MD[8], Antoine Martin, MD[9,10], Regis Cohen, MD[11,12], Susan Richter, PhD[13], Judith Balmaña, MD, PhD[14], Esther Korpershoek, PhD[15], Elena Rapizzi, PhD[16], Timo Deutschbein, MD[17], Laurent Vroonen, MD[18], Judith Favier, PhD[2], Ronald R. de Krijger, MD, PhD[19,20], Martin Fassnacht, MD, PhD[17], Felix Beuschlein, MD[21,22], Henri J. Timmers, MD, PhD[23], Graeme Eisenhofer, PhD[13,24], Massimo Mannelli, MD, PhD[16], Karel Pacak, MD, PhD[25], Jorgina Satrústegui, PhD[5,6], Cristina Rodríguez-Antona, PhD[1,6], Laurence Amar, MD, PhD[2,26], Alberto Cascón, PhD[1,6], Nicole Dölker, PhD[3], Anne-Paule Gimenez-Roqueplo, MD, PhD[2,27] and Mercedes Robledo, PhD[1,6]

[1]Hereditary Endocrine Cancer Group, Spanish National Cancer Research Centre (CNIO), Madrid, Spain. [2]INSERM, UMR970, Paris Cardiovascular Research Center and Université Paris Descartes, Sorbonne Paris Cité, Faculté de Médecine; Equipe labellisée Ligue contre le cancer, Paris, France. [3]Structural Biology and BioComputing Programme, Spanish National Cancer Research Centre (CNIO), Madrid, Spain. [4]Department of Immunology and Oncology, National Centre for Biotechnology (CNB-CSIC), Madrid, Spain. [5]Departamento de Biología Molecular, Centro de Biología Molecular Severo Ochoa UAM-CSIC, Universidad Autónoma de Madrid and Instituto de Investigación Sanitaria Fundación Jiménez Díaz, Madrid, Spain. [6]Centro de Investigación Biomédica en Red de Enfermedades Raras (CIBERER), Madrid, Spain. [7]Department of Endocrinology and Nutrition Service, Hospital Universitario 12 de Octubre, Madrid, Spain. [8]Servicio Oncología Médica, Hospital Infanta Leonor, Vallecas, Madrid, Spain. [9]Assistance Publique Hôpitaux de Paris; Hôpital Avicenne, Service d'anatomie et cytologie pathologiques, Bobigny, France. [10]INSERM, U978, Université Paris 13, Sorbonne Paris Cité, Bobigny, France. [11]Assistance Publique-Hôpitaux de Paris, Hôpital Avicenne, Service de Médecine Interne, Bobigny, France. [12]Université Paris 13, Sorbonne Paris Cité, Bobigny, France. [13]Institute of Clinical Chemistry and Laboratory Medicine, University Hospital Carl Gustav Carus, Medical Faculty Carl Gustav Carus, Technische Universität Dresden, Dresden, Germany. [14]High Risk and Cancer Prevention Group, Medical Oncology Department, Vall d'Hebron University Hospital and Vall d'Hebron Institute of Oncology, Barcelona, Spain. [15]Department of Pathology, Erasmus Medical Center Cancer Institute, University Medical Center Rotterdam, Rotterdam, The Netherlands. [16]Department of Experimental and Clinical Medicine, University of Florence, Florence, Italy. [17]Department of Internal Medicine I, Division of Endocrinology and Diabetes, University Hospital, University of Würzburg, Würzburg, Germany. [18]Department of Endocrinology, Centre Hospitalier Universitaire (CHU) de Liège, Liège, Belgium. [19]Department of Pathology, Erasmus University Medical Center, Rotterdam, The Netherlands. [20]Department of Pathology, Reinier de Graaf Hospital, Delft, The Netherlands. [21]Medizinische Klinik und Poliklinik IV, Klinikum der Universität München, Ludwig-Maximilians-Universität München, Munich, Germany. [22]Klinik für Endokrinologie, Diabetologie und Klinische Ernährung, Universitätsspital Zürich, Zürich, Switzerland. [23]Department of Internal Medicine, Radboud University Medical Centre, Nijmegen, The Netherlands. [24]Department of Medicine III, University Hospital and Medical Faculty Carl Gustav Carus, Dresden University of Technology, Dresden, Germany. [25]Section on Medical Neuroendocrinology, Eunice Kennedy Shriver National Institute of Child Health and Human Development, NIH, Bethesda, Maryland, USA. [26]Assistance Publique-Hôpitaux de Paris, Hôpital Européen Georges Pompidou, Hypertension Unit, Paris, France. [27]Assistance Publique-Hôpitaux de Paris, Hôpital Européen Georges Pompidou (HEGP), Department of Genetics, Paris, France.